Title

Chromophore-Based Luminescent Metal—Organic Frameworks as Lighting Phosphors

Journal

Inorganic Chemistry, 55(15)

ISSN

0020-1669

Authors

Lustig, William P

Wang, Fangming

Teat, Simon J

et al.

Publication Date

2016-08-01

DOI

10.1021/acs.inorgchem.6b00897

Peer reviewed

Chromophore-based Luminescent Metal–Organic Frameworks (LMOFs) as Lighting Phosphors

William P. Lustig,[†,∥] Fangming Wang,[†,∥,¶] Simon J. Teat,[‡] Zhichao Hu,[†] Qihan Gong,[†] and Jing Li[†,*]

[†]Department of Chemistry and Chemical Biology, Rutgers University, 610 Taylor Road, Piscataway, New Jersey 08854, United States

[‡]Advanced Light Source, Lawrence Berkeley National Laboratory, 1 Cyclotron Road, Berkeley California 94720, United States

ABSTRACT: Energy-efficient solid state lighting (SSL) technologies are rapidly developing, but the lack of stable, high performance rare-earth free phosphors may impede the growth of the SSL market. One possible alternative is organic phosphor materials, but these can suffer from lower quantum yields and thermal instability when compared to rare-earth phosphors. However, if luminescent organic chromophores can be built into a rigid metal-organic framework, their quantum yields and thermal stability can be greatly improved. This highlight article discusses the design of a group of such chromophore-based luminescent metal-organic frameworks (LMOFs) with exceptionally high performance, and rational control of the important parameters that influence their emission properties, including electronic structures of chromophore, co-ligands, metal ions, and guest molecules.

1. INTRODUCTION

As global awareness of the importance of energy efficiency has increased, solid state lighting devices have been rapidly adopted because of their low power usage and long lifetimes. According to the 2015 US Department of Energy SSL Research & Development Plan, light-emitting diode (LED)-based bulbs made up only 5% of global sales in 2014, but are expected to comprise 42% of global sales by 2020.[1] In the United States, it is estimated that 88% of all general lighting devices will be LED-based by 2030, saving between 260 and 395 terawatt-hours of energy annually. To provide some perspective, that is almost twice the projected 2030 annual electrical energy output for wind and solar energy combined.[1]

Currently, most white LEDs fall into two categories: multi-chip white LEDs (MC-WLEDs), in which white light is created by mixing emission from red, green, and blue LED chips,[2] or phosphor-converted white LEDs (PC-WLEDs), in which white light is created by mixing emission from a blue or UV LED chip with emission from yellow or red/green/blue phosphors, respectively.[3] Because of their relative simplicity, blue/yellow PC-WLEDs are the most efficient.[4] A cerium(III)-doped yttrium-aluminum garnet (YAG:Ce) is the most commonly used yellow phosphor in these PC-WLEDs, but this presents a challenge. The global supply of yttrium is projected to remain at a deficit relative to demand until beyond 2020, and more than 99% of worldwide yttrium deposits are located in China.[5] As the demand for yttrium and other rare-earth metals increases, new rare-earth free phosphor materials must be developed in order to reach projected LED adoption levels.[6]

Organic phosphors are one possible alternative, although yellow and red emitting organic chromophores typically suffer from lower quantum yields and thermal instability when compared to rare-earth phosphors such as YAG:Ce. One way to address this challenge is to construct robust

structures by incorporating these organic chromophores into metal-organic frameworks (MOFs).

MOFs are structures built of single metal ions (primary building units or PBUs) or metal ion clusters (secondary building units or SBUs) that are linked together in an ordered fashion by organic ligands. Many MOFs exhibit permanent porosity, and their chemical and physical properties can be tuned by altering the metal ion(s) or organic ligand(s) that they are composed of. Because of their easy-to-functionalize pore surfaces and diverse structures, MOFs are being investigated for a variety of applications, including gas storage and separation, catalysis, and sensing,[7-8]

Our strategy to develop organic chromophore-based MOFs is centered on the following consideration: By using chromophoric ligands in the synthesis, highly luminescent metal-organic frameworks (LMOFs) can be constructed that not only can maintain the emission from their ligands but also enhance and tune their emission properties. LMOF quantum yields (QYs) can be higher than their chromophoric ligands because their rigid structures limit the molecular vibrations, torsions, and rotations that often lead to nonradiative excitation decay in the molecular chromophore.[9] In addition, binding chromophores into a rigid framework can improve their thermal stability. Third, including a second ligand in the framework construction may contribute to fine-tuning of emission energy and color. Finally, as many MOFs are porous, it also provides an opportunity to tailor chromophore emission via host-guest interactions.

2. OVERVIEW OF LMOF DESIGN AND SYNTHESIS

2.1. LMOF-231 In order to design a high performing LMOF, we began by selecting a strongly emissive organic chromophore that could be functionalized with carboxylate groups to provide binding sites for its eventual construction into a framework structure. Our starting point was the chromophore tetraphenylethene (tpe), which is well-known to fluoresce through aggregation-induced emission (AIE).[10] An AIE chromophore was initially chosen because it was known that restricting the molecular movement available to the chromophore would result in markedly improved luminescent efficiency (such a restriction should occur upon incorporation into a framework); however, this process is generalizable to non-AIE chromophores as well.[11]

One drawback of using tpe as the chromophore in constructing an LMOF is its high emission energy.[9] As described above a blue-excitable, yellow-emitting LMOF would be preferable for use in PC-WLEDs, and the chromophore emission should be consistent with that goal. In order to shift the emission into the yellow region, DFT calculations (see S2) were performed to estimate the impact of structural changes to the tetracarboxylated tpe chromophore tetrakis(4-carboxyphenyl)ethylene (H_4tcpe) on its emission energy (table 1). These calculations indicated that the extension of each H_4tcpe arm by an additional phenyl ring should redshift the molecule's emission energy. This led to the synthesis of a yellow chromophore 1,1,2,2-tetrakis(4-(4-carboxy-phenyl)phenyl)ethene (H_4tcbpe) (fig. 1). As desired, H_4tcbpe exhibits strong yellow emission at 540 nm, with a high

Table 1. Calculated HOMO/LUMO energy levels and estimated band gap of chromophores, co-ligands, and LMOF fragments.

Species	HOMO (eV)	LUMO (eV)	ΔE (eV)
H_4tcpe	-6.40	-2.68	3.72
H_4tcbpe	-5.87	-2.46	3.41
H_4(tcbpe-F)	-6.10	-2.68	3.42
tppe	-6.03	-2.25	3.78
btc	-8.19	-2.53	5.66
azpy	-7.15	-3.34	3.81
bpe	-7.24	-1.17	6.07
3 fragment	-6.01	-2.48	3.53

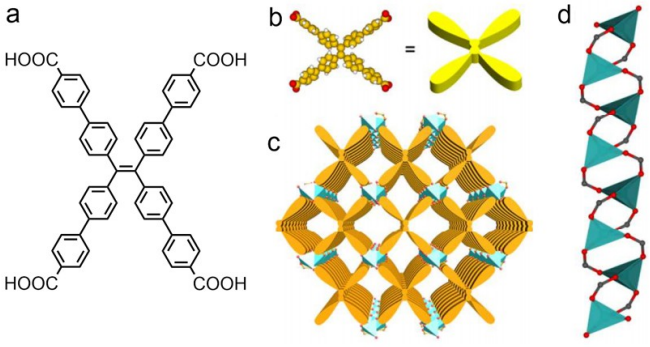

quantum yield of 70.3% under 365 nm excitation (fig. 2).

Figure 1. (a) The structure of H_4tcbpe. (b) The simplified representation of the tcbpe ligand. (c) The structure of **1'**, viewed along the *c* axis, demonstrating the pi-pi stacking of the tcbpe ligand. (d) A view of the tetrahedrally-coordinated Zn infinite PBU, with two carboxylate groups bridging between each of the Zn^{2+} ions, viewed from the *b* axis. The Zn^{2+} ion is the blue tetrahedron, oxygen atoms are red, and carbon atoms are grey.

Finally, in designing a LMOF with chromophore-based emission, it was important that the metal ions used in constructing the framework do not interfere with the chromophore's optical properties. The Zn^{2+} ion was chosen for this purpose, as density of states (DOS) calculations indicate that the fully occupied

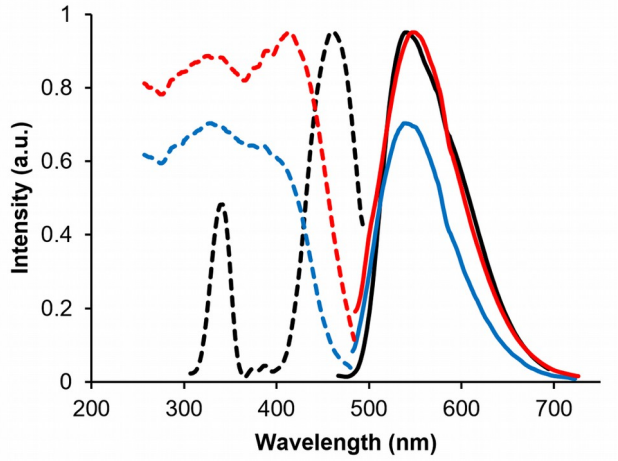

3d subshell lies far below the valence band (VB) region, preventing the metal ion from participating in MOF luminescence (See S2, figure S2).[12]

Figure 2. The excitation (dotted) and emission (solid) spectra for the H_4tcbpe chromophore (blue), **1'** (red), and the commercial phosphor YAG:Ce (black). Peak emission and excitation intensity is scaled to internal quantum yield. Reproduced from reference listing #13. Copyright 2015, Royal Society of Chemistry.

LMOF-231, with the formula Zn_2(tcbpe)·*x*DMA (**1**), was synthesized in solvothermal conditions; 0.3 mmol $Zn(NO_3)_2·6H_2O$ reacted with 0.03 mmol H_4tcbpe in 2 mL DMA at 120 °C for 48 hours.[13] The residual solvent molecules were then removed by heating under vacuum at 100 °C overnight to give **1'**, with structural stability confirmed *via* powder X-ray diffraction (see S6, figure S4). The structure is composed of an infinite zinc-carboxylate primary building unit (PBU) running in the *c* direction, with stacked columns of tcbpe molecules bridging four zinc-carboxylate chains. The zinc ions are tetrahedrally coordinated, with two carboxylates bridging between each Zn^{2+} ion and its two

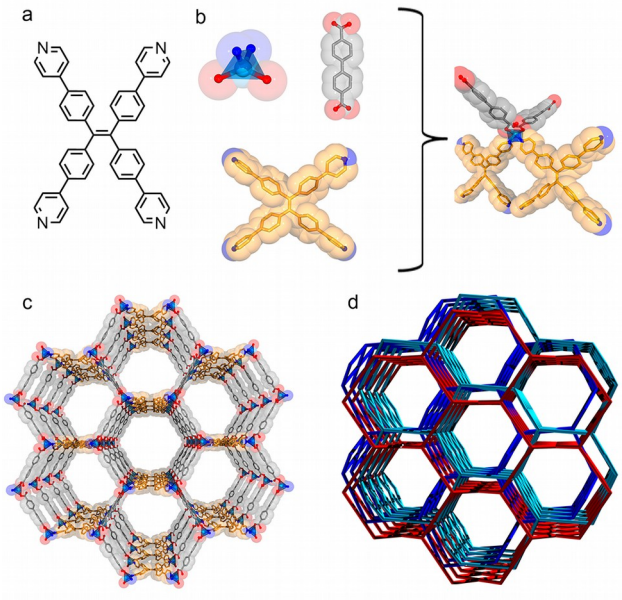

neighboring ions. The tcbpe layers are closely packed, with interlayer H-H distances between 2.4 and 3.2 Å (fig. 1).

1' has exceptional optical properties; its performance clearly demonstrates the value of incorporating the H_4tcbpe chromophore into a metal-organic framework. While maintaining the H_4tcbpe's desirable emission energy with only a slight redshift to 550 nm, the immobilization of the molecule enforced by the framework increased the internal quantum yield from 70.3% under 365 nm excitation for the bulk chromophore to 82.5% for the solvated framework **1** by preventing phenyl ring rotation and C=C bond torsion at the central ethene moiety, which dominate non-radiative excitation decay pathways in tpe-based chromophores.[14] Outgassing to yield **1'** eliminates emission-quenching due the solvent molecules, further increasing the internal quantum yield to 95.1% under 365 nm excitation and 76.4% under 455 nm excitation, which is competitive with the commercial phosphor YAG:Ce (fig. 2).

In addition to improving the chromophore's optical qualities, incorporating H_4tcbpe into a metal-organic framework significantly enhanced its thermal stability, as indicated by thermogravimetric (TG) analysis (see S7, fig. S7). While molecular

H_4tcbpe began to decompose around 340 °C, **1'** remained thermally stable until about 450 °C.

2.2. LMOF-241 In addition to carboxylate-based chromophores like H_4tcbpe, chromophores with appropriately positioned pyridine groups (and other nitrogen-based groups) can also be incorporated into LMOFs. However, in order to construct a neutral framework using a pyridine-based ligand, a secondary carboxylate-based ligand is needed for charge balancing. We constructed an example of this type of LMOF using the pyridine derivative of H_4tcbpe, which is 1,1,2,2-tetrakis(4-(pyridin-4-yl)phenyl)ethene (tppe) (fig. 3), synthesized according to a method we reported.[15] Bulk tppe emits at 490 nm under 340 nm excitation, with an internal quantum yield of 76.7% The secondary carboxylate ligand chosen for this structure is [1,1'-biphenyl]-4,4'-dicarboxylic acid (bpdc). As in the previous case and for the same reasons, the Zn^{2+} ion was used to immobilize the tppe and bpdc into a rigid framework.

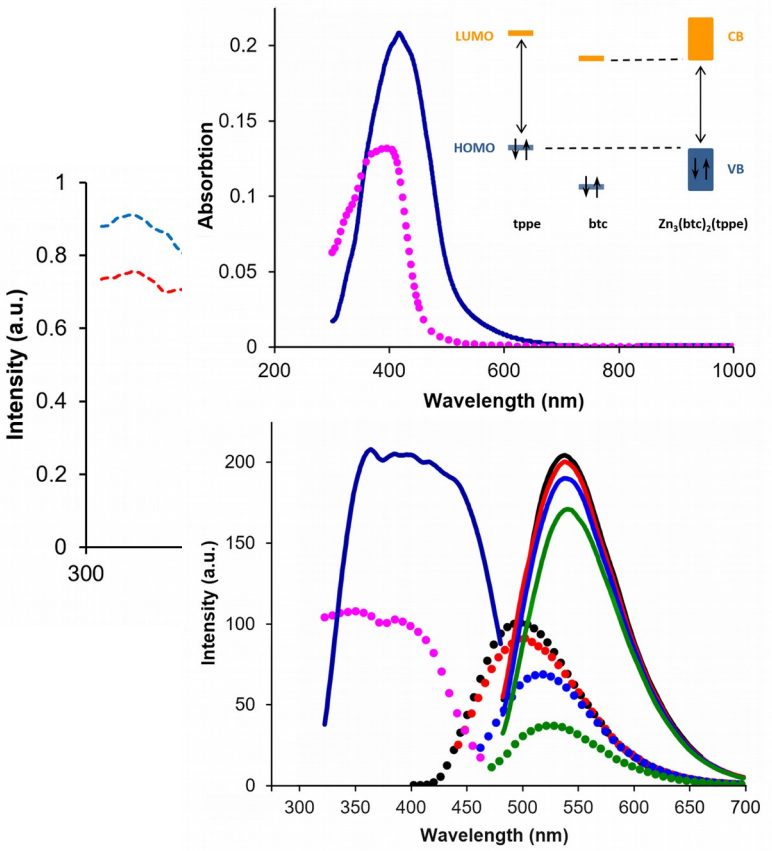

Figure 3. (a) The structure of the chromophore tppe. (b) The tetrahedral Zn^{2+} ion, bpdc co-ligand in grey, and tppe in gold combining to form the PBU. (c) Structure of a single LMOF-241 framework, with hexagonal channels running along the *c* axis. (d) Three distinct LMOF-241 frameworks which interpenetrate to form the complete structure. Color scheme: key: C, grey or gold; N, blue; O, red; Zn, aqua. Reprinted with permission from reference 15. Copyright 2015 American Chemical Society.

LMOF-241 (**2**), with the formula $Zn_2(bpdc)_2(tppe)\cdot sol$ (sol = solvent molecules), was synthesized in solvothermal conditions, with 0.05 mmol $Zn(NO_3)_2\cdot 6H_2O$ reacting with 0.02 mmol tppe and 0.05 mmol bpdc in 12 mL 4:1:1 DMA:dismethylsulfoxide (DMSO):isopropyl alcohol (IPA) at 150 °C for 24 hours. Following solvent exchange with dichloromethane (DCM), the structure was outgassed under vacuum overnight at 60 °C, with powder X-ray diffraction (PXRD) analysis used to confirm the stability of the structure following outgassing (see S6, figure S5). This structure is composed of three interpenetrated frameworks, with each framework consisting of tetrahedrally coordinated Zn^{2+} PBUs linked to its neighbors by two bridging tppe ligands and two bridging bpdc ligands. Hexagonal channels run along the *c* axis of each framework, and remain present (though distorted) in the triply interpenetrated final structure (fig. 3). As observed with **1'**, the emission from the chromophore tppe is preserved in **2** with only a slight redshift of 10 nm (from 490 nm to 500 nm), while the internal quantum yield is increased from 76.7% to 92.7% under 340 nm excitation (fig. 4).

Figure 4. The excitation spectra (dotted) and emission spectra (solid) for the tppe chromophore (red) and **2** (blue). Peak intensity is scaled to internal quantum yield. Reprinted with permission from reference 15. Copyright 2015 American Chemical Society.

2.3. LMOF-251 Beyond serving structural and charge-balancing needs, secondary ligands can also participate in luminescence via a ligand-to-ligand charge transfer mechanism,[16] presenting an opportunity to adjust the emission energy from the primary chromophore ligand. In the previous examples, we were interested in keeping the chromophore emission essentially unchanged, so the metal and co-ligand were chosen specifically to avoid interacting optically with the chromophore ligand. As a result, the LMOF HOMO/LUMO energy levels reflected solely those of the

chromophores. However, if we use a co-ligand with a LUMO energy level that is lower than that of the chromophore, the LUMO of the LMOF should also be lower, resulting in redshifted emission (fig. 5). This process of bandgap modulation is especially interesting in the case of tppe, since the green-emitting chromophore would have more applications if its emission could be tuned into the yellow region.

Figure 5. Top: UV-Vis absorption of tppe (pink, dotted) and **3** (blue, solid). Inset is a schematic demonstrating the relative positions of the HOMO/LUMO energy levels of tppe, btc, and **3**, and the bandgap modulation process. Bottom: The excitation and emission spectra of the tppe chromophore (dotted) and **3** (solid), with emission spectra collected under varying excitation energies. tppe: excitation (pink), emission under 360 nm (black), 400 nm (red), 420 nm (blue), 440 nm (green). **3**: excitation (blue, left), emission under 360 nm (black), 400 nm (red), 420 nm (blue, right), 440 nm (green). Reprinted with permission from reference 17. Copyright 2014 American Chemical Society.

To realize this emission shift, we synthesized a LMOF containing tppe and benzene-1,3,5-tricarboxylic acid (btc).[17] DFT calculations (see S2) indicated that the LUMO of btc lies approximately 0.279 eV below that of tppe (table 1), enabling its use as a bandgap modulator for tppe. LMOF-251 (**3**), with the formula $Zn_3(btc)_2(tppe)(DMA)\cdot 4.5DMA\cdot 6H_2O$, was synthesized with 0.06 mmol $Zn(NO_3)_2\cdot 6H_2O$, 0.04 mmol btc, 0.02 mmol tppe, and 0.3 mL concentrated tetrafluoroboric acid in 15 mL DMA at 150 °C for 48 hours. The resulting LMOF is comprised of two interpenetrated frameworks (fig. 6d), with each framework containing both tetrahedrally coordinated zinc PBUs and zinc paddlewheel SBUs. Each of the paddlewheel SBUs contains two zinc ions bridged by four carboxylate groups from btc ligands, with a molecule of water coordinated to each zinc along the paddlewheel axis. Each paddlewheel is connected to two neighboring SBUs (one above and one below) by the remaining btc carboxylates through four PBUs, forming a chain that runs along the *a* axis. Each PBU is also coordinated to two tppe molecules lying in the *bc* plane, with each tppe linking two of these chains together (fig. 6).

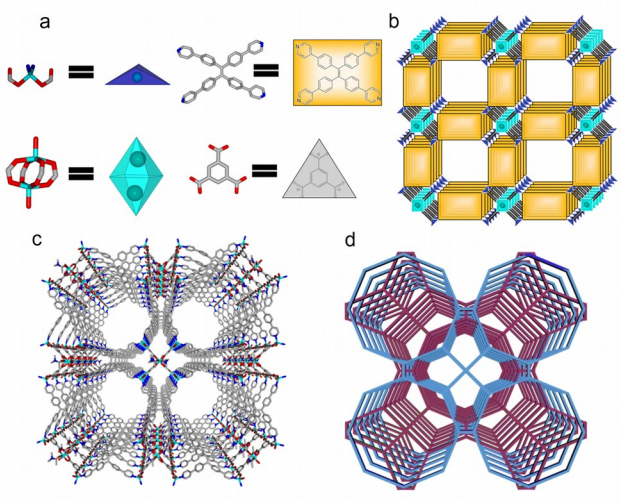

Figure 6. (a) Schematic representations of the PBU (top left), tppe chromophore (top right), SBU (bottom left), and btc ligand (bottom left). (b) The structure of a single net in **3**, with large octagonal channels running along the-*a* axis. (c) View along the *a*-axis showing 1D channels in the framework. (d) Two identical frameworks interpenetrate to form the complete structure of **3**. Color scheme: key: C, grey; N, blue; O, red; Zn, aqua. Reprinted with permission from reference 17. Copyright 2014 American Chemical Society.

As desired, **3** emits strongly in the yellow region at 540 nm (fig. 5, bottom), corresponding to a redshift of approximately 50 nm compared to the tppe chromophore (btc is not fluorescent in the visible range). The expected reduction in the bandgap that is responsible for this redshifted emission is supported by UV-Vis reflectance spectroscopy, which indicates that the bandgaps of tppe and **3** are approximately 2.7 and 2.4 eV, respectively (fig. 5, top). To further confirm the reduced bandgap of **3** when compared to tppe and the role of btc in bandgap modulation, DFT calculations were used to estimate the orbital energy levels of a neutral fragment of the LMOF (see S2, fig. S2). The HOMO energy level of **3** was calculated to be only 0.02 eV lower than that of tppe while its LUMO was 0.23 eV lower, which is in trend with experimental data. Additionally, the LUMO of **3** was calculated to be within 0.05 eV of btc's LUMO, confirming the bandgap modulating role of btc (table 1).

As in previous cases, immobilizing the chromophore greatly improved the material's internal quantum yield, which was increased from to 57.2% to 90.7% under 400 nm excitation. Additionally, the bandgap modulation greatly improved the ability of **3** to be excited by blue light relative to tppe (fig. 6). Under 420 nm excitation, the quantum yield improved from 40.2% in tppe to

72.9% in **3**; under 450 nm excitation, the improvement was from 32.1% to 63.9%.

2.4. LMOF-302 In order to investigate the impact of structural changes on chromophore performance, we sought to incorporate pyridine-based co-ligands intro structures containing the fluorinated H_4tcbpe analog, H_4tcbpe-F (fig. 7). Being fluorinated at the ortho position relative to the carboxylic acid group, it was hoped that the fluorine would moderately reduce electron density on the carboxylate groups, thereby reducing the electron density available for coordination to the Zn^{2+} ions, making the Zn^{2+} in turn more amenable to coordination with the pyridine lone pair. Additionally, DFT calculations (see S2) indicated that while functionalization with fluorine would decrease the chromophore's HOMO and LUMO energy levels, the chromophore's HOMO/LUMO gap should be essentially unchanged (table 1). As expected, the fluorinated ligand fluoresced at 540 nm under 455 nm excitation, which is identical to the non-fluorinated ligand. However, while the emission energy was unchanged, the internal quantum yield of H_4tcbpe-F is only 46.5% under 455 nm excitation, as compared to 62.3% for H_4tcbpe. Despite this decrease, the H_4tcbpe-F chromophore is still an effective model with which to study structural effects on chromophore behavior.

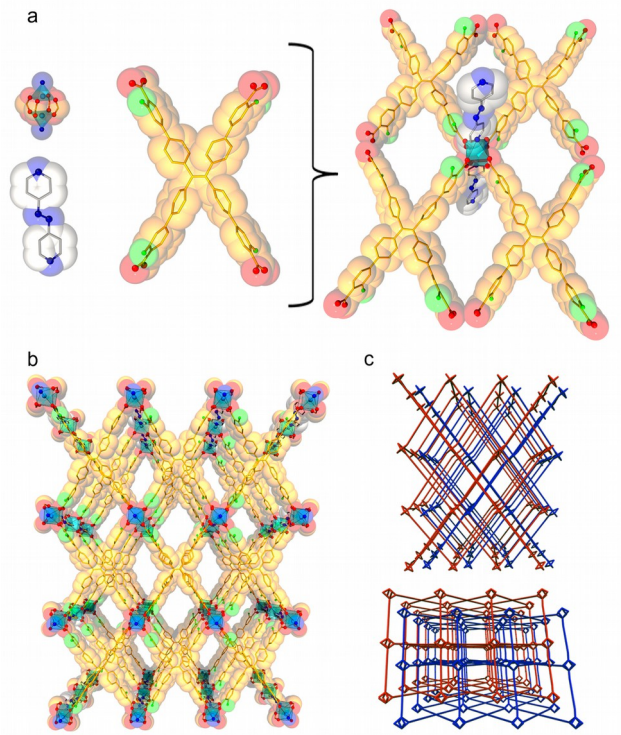

Figure 7. (a) Zinc paddlewheel (top left), azpy co-ligand (bottom left), and tcbpe-F fluorophore combining to form a fragment of **4**. (b) Structure of a single framework in **4**, viewed along the *b*-axis. (c) Two identical frameworks interpenetrate to form the complete structure of **4**, viewed along the *b* (top) and *c* (bottom) axes. Color scheme: key: C, grey or gold; N, blue; O, red; F, green; Zn, aqua.

Following synthesis of H_4tcbpe-F (see S3), the first pyridine ligand to be incorporated into a structure with H_4tcbpe-F was 4,4'-azopyridine (azpy). 0.05 mmol azpy was introduced into solution with 0.05 mmol H_4tcbpe-F and 0.10 mmol $Zn(NO_3)_2 \cdot 6H_2O$ in DMA. Following 48 hours at 100 °C, the non-fluorescent crystalline product LMOF-302 (**4**) with formula Zn_2(tcbpe-F)(azpy) was recovered. Single crystal X-ray analysis (see S4, table S1) showed that the resulting structure is formed by two interpenetrated frameworks, which are related to each other through a center of inversion. Each framework consists of the classic Zn^{2+} paddlewheel SBUs, in which two Zn^{2+} atoms are bridged by four roughly orthogonal carboxylate groups from tcbpe-F. These SBUs are each coordinated to four tcbpe-F molecules, which are in turn coordinated to four more SBUs (etc.), forming a two-dimensional sheet in the *ac* plane. These sheets are linked by pillaring azpy ligands in the *c* direction, which coordinate through the pyridyl nitrogen and connect each of the SBUs to those above and below (fig. 7).

As shown by thermogravimetric analysis (TGA), **4** decomposes at approximately 330 °C, which is 120 °C lower than **1** (see S7, fig. S7). A decrease in thermal stability is to be expected when comparing **1** and **4**, as the SBUs in **4** contain Zn-N bonds, which are relatively weaker than the Zn-O bonds which make up the entirety of ligand-metal bonds in **1**.[18] Additionally, the high degree of tcbpe pi-pi stacking in **1** increases its thermal stability, whereas gaps of approximately 5.7 Å separate every two layers of tcbpe-F in **4**, limiting the effectiveness of the pi-pi stacking as a thermal stabilization mechanism.

2.5. LMOF-304 The second pyridine-based ligand to be incorporated into a structure with tcbpe-F was 1,2-bis(4-pyridyl)ethane (bpe). Under the same reaction conditions as **4** (but with bpe replacing azpy), the crystalline product Zn_2(tcbpe-F)(bpe)·*n*DMA was recovered. PXRD was used to

confirm that the product is isoreticular with **4** (fig. 8). Solvent exchange with acetone was performed to remove residual DMA from the pores, followed by outgassing under vacuum. TGA was used to confirm the full removal of the solvent, giving LMOF-304

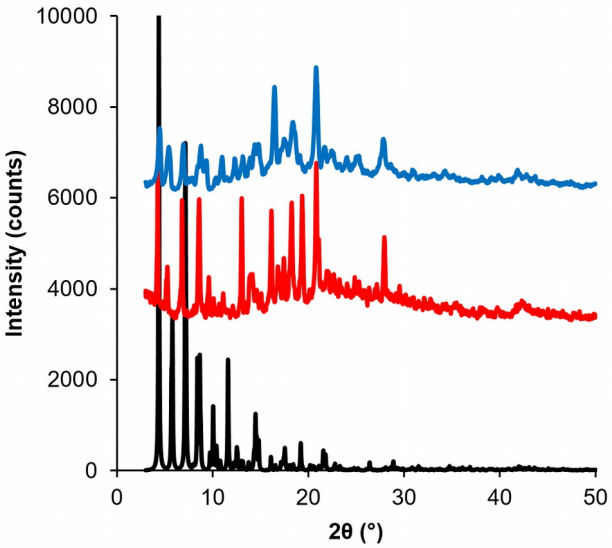

(**5**), with the formula Zn_2(tcbpe-F)(bpe) (see S7, fig. S8).

Figure 8. Overlaid PXRD patterns for **4** (red) and **5** (blue). The simulated pattern for **4** is in black.

Unlike **4**, **5** is strongly luminescent, with a peak emission of 527 nm and an internal quantum yield of 64.0% under 455 nm excitation (fig. 9). This increase from 46.5% in the fluorinated chromophore H_4tcbpe-F to 64% in **5** is commensurate with the increased quantum yields observed between H_4tcbpe and **1**, suggesting that the lower quantum yield of **5** when compared to **1** is due primarily to the lower quantum yield of H_4tcbpe-F, rather than being due to some structural factor. This consistency in the face of structural differences implies that it is possible to significantly alter LMOF structures and connectivity without affecting the base chromophore luminescence. The result also suggests that introducing a co-ligand can alter the electronic structure and consequently, tune the emission energy, of a LMOF.

Figure 9. The excitation spectra (dotted) and emission spectra (solid) for the tcbpe-F chromophore (blue) and **5** (red). Peak excitation and emission intensity is scaled to internal quantum yield.

In addition to the positive influences that incorporating a chromophore into a MOF has on fluorescence quantum yield and stability, MOFs can

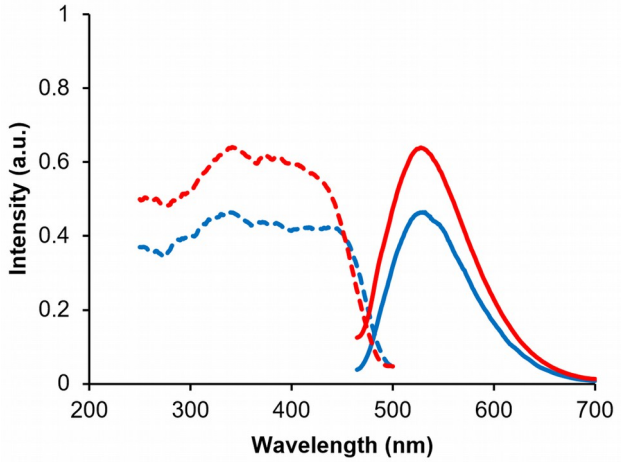

often possess permanent porosity. This presents an opportunity to further influence LMOF emission through loading guest molecules into the structure.

In order to investigate the influence that potential host-guest interactions could have on emission from **5**, aromatic solvents with varying functional groups were loaded into this LMOF using a solvent-exchange procedure (see S8, fig. S9). Under 365 nm excitation, the emission from **5** was tunable based on which guest molecule was present (fig. 10).

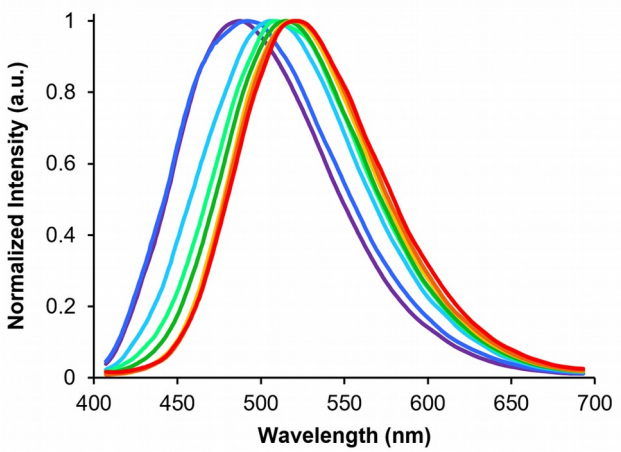

Figure 10. Overlaid normalized emission spectra for guest-loaded samples of **5**. In order of decreasing emission energy, the guest molecules are: Butylbenzene (violet), 1,2,4-Trimethylbenzene (blue), p-Chlorotoluene (aqua), p-Xylene (light green), Bromobenzene (dark green), Chlorobenzene (yellow), Toluene (orange), and outgassed **5** (red, no guest molecule).

Interestingly, the electron donating or withdrawing character of functional groups on the guest molecules had little effect on the observed emission shift; instead, guest molecule size appears to have had the

largest impact. In the presence of butylbenzene and 1,3,5-trimethylbenzene, emission from **5** was strongly blueshifted to 488 and 489 nm, respectively. A more moderate blueshift was observed in the presence of p-chlorotoluene and p-Xylene, with emission at 508 and 509 nm, while the smallest blueshift was observed in the presence of bromobenzene, chlorobenzene, and toluene, with emission peaks at 517, 519, and 520 nm. This relationship between guest size and emission shifting may be related to the closer interactions that are expected between larger guest molecules and the LMOF pore.

3. CONCLUSIONS AND OUTLOOK

Chromophore-based LMOFs present an exciting opportunity to develop high-performance, rare-earth free phosphor materials. Upon immobilizing organic chromophores into a rigid framework, both their luminescence quantum efficiency and thermal stability can be greatly improved. Various LMOF structures can be obtained by incorporating different chromophores, and adjustments to the chromophore emission energy can be achieved through the careful selection of co-ligands. Additionally, the inherent porosity of the LMOF system presents the opportunity to further tune phosphor emission through the interaction with selected guest molecules.

In this Highlight article, we have briefly discussed the process of constructing several highly emissive LMOFs with potential applications as lighting phosphor materials and presented two new isoreticular MOFs with varying luminescence properties. Future work in this area will include more in-depth studies of the fluorescence mechanism in dual-ligand MOFs, as well as an effort to develop LMOFs based on orange and red emitting organic chromophores.

■ ASSOCIATED CONTENT

Supporting Information

The supporting information is available free of charge on the Inorganic Chemistry website at DOI: XXXXXXXXX.

Materials used

Instrumentation descriptions

DFT calculation parameters

Ligand synthesis

Single crystal data

Powder X-ray diffraction data

Thermogravimetric analyses

Solvent exchange procedures

■ AUTHOR INFORMATION

Corresponding Author

* jingli@rutgers.edu

Present Addresses

¶ School of Environmental and Chemical Engineering, Jiangsu University of Science and Technology, Zhenjiang, Jiangsu 212003, P.R. China

Author Contributions

‖ WPL and FW contributed equally to this work.

Notes

The authors declare no competing financial interest.

■ ACKNOWLEDGEMENTS

We are grateful for the financial support from the National Science Foundation (Grant No. DMR-1507210) to carry out this work. The Advanced Light Source (ALS) is supported by the Director, Office of Science, Office of Basic Energy Science, of the U.S. Department of Energy, under contract DE-AC02-05CH11231.

■ REFERENCES

1. Bardsley, N.; Bland, S.; Hansen, M.; Pattison, L.; Pattison, M.; Stober, K.; Yamada, M. *Solid State Lighting R&D Plan*; US Department of Energy: 2015.

2. Yin, L.; Yang, L.; Yang, W.; Guo, Y.; Ma, K.; Li, S.; Zhang, J., *Solid-State Electron.* **2010,** *54*, 1520-1524.

3. (a) Dabre, K. V.; Dhoble, S. J., *JOL* **2014,** *150*, 55-58; (b) Pust, P.; Weiler, V.; Hecht, C.; Tücks, A.; Wochnik, A. S.; Henß, A.-K.; Wiechert,

D.; Scheu, C.; Schmidt, P. J.; Schnick, W., *Nat. Mater.* **2014,** *13*, 891-896.

4. Pimputkar, S.; Speck, J. S.; DenBaars, S. P.; Nakamura, S., *Nat. Photonics* **2009,** *3*, 180-182.

5. *Report on Critical Raw Materials for the EU: Critical Raw Materials Profiles*; European Commission: 2014.

6. *Energy Savings Forecast of Solid-State Lighting in General Illumination Applications*; US Department of Energy: 2014.

7. (a) Zhang, Z.; Zhao, Y.; Gong, Q.; Li, Z.; Li, J., *Chem. Commun.* **2013,** *49*, 653-661; (b) Wu, H.; Gong, Q.; Olson, D. H.; Li, J., *Chem. Rev.* **2012,** *112*, 836-868; (c) Cui, Y.; Song, R.; Yu, J.; Liu, M.; Wang, Z.; Wu, C.; Yang, Y.; Wang, Z.; Chen, B.; Qian, G., *Adv. Mater.* **2015,** *27*, 1420-1425; (d) Qin, J.; Ma, B.; Liu, X.-F.; Lu, H.-L.; Dong, X.-Y.; Zang, S.-Q.; Hou, H., *J. Mater. Chem. A* **2015,** *3*, 12690-12697; (e) Stavila, V.; Parthasarathi, R.; Davis, R. W.; El Gabaly, F.; Sale, K. L.; Simmons, B. A.; Singh, S.; Allendorf, M. D., *ACS Catal.* **2016,** *6*, 55-59; (f) Zhu, X.; Zheng, H.; Wei, X.; Lin, Z.; Guo, L.; Qiu, B.; Chen, G., *Chem. Commun.* **2013,** *49*, 1276-1278; (g) Zhang, Y.-B.; Furukawa, H.; Ko, N.; Nie, W.; Park, H. J.; Okajima, S.; Cordova, K. E.; Deng, H.; Kim, J.; Yaghi, O. M., *J. Am. Chem. Soc.* **2015,** *137*, 2641-2650; (h) Hu, T.-L.; Wang, H.; Li, B.; Krishna, R.; Wu, H.; Zhou, W.; Zhao, Y.; Han, Y.; Wang, X.; Zhu, W.; Yao, Z.; Xiang, S.; Chen, B., *Nat. Commun.* **2015,** *6*, 7328; (i) Feng, D.; Gu, Z.-Y.; Li, J.-R.; Jiang, H.-L.; Wei, Z.; Zhou, H.-C., *Angew. Chem.* **2012,** *124*, 10453-10456.

8. (a) Hu, Z.; Deibert, B. J.; Li, J., *Chem. Soc. Rev.* **2014,** *43*, 5815-5840; (b) Allendorf, M. D.; Bauer, C. A.; Bhakta, R. K.; Houk, R. J. T., *Chem. Soc. Rev.* **2009,** *38*, 1330-1352; (c) Cui, Y.; Yue, Y.; Qian, G.; Chen, B., *Chem. Rev.* **2012,** *112*, 1126-1162.

9. Shustova, N. B.; McCarthy, B. D.; Dincă, M., *J. Am. Chem. Soc.* **2011,** *133*, 20126-20129.

10. (a) Han, X.; Liu, D.-E.; Wang, T.; Lu, H.; Ma, J.; Chen, Q.; Gao, H., *ACS Appl. Mater. Interfaces* **2015,** *7*, 23760-23766; (b) Iasilli, G.; Battisti, A.; Tantussi, F.; Fuso, F.; Allegrini, M.; Ruggeri, G.; Pucci, A., *Macromol. Chem. Phys.* **2014,** *215*, 499-506; (c) Tong, H.; Hong, Y.; Dong, Y.; Hau; Lam, J. W. Y.; Li, Z.; Guo, Z.; Guo, Z.; Tang, B. Z., *Chem. Commun.* **2006**, 3705-3707.

11. Mei, J.; Leung, N. L. C.; Kwok, R. T. K.; Lam, J. W. Y.; Tang, B. Z., *Chem. Rev.* **2015,** *115*, 11718-11940.

12. (a) Banerjee, D.; Hu, Z.; Pramanik, S.; Zhang, X.; Wang, H.; Li, J., *CrystEngComm* **2013,** *15*, 9745-9750; (b) Pramanik, S.; Hu, Z.; Zhang, X.; Zheng, C.; Kelly, S.; Li, J., *Chem. - Eur. J.* **2013,** *19*, 15964-15971; (c) Pramanik, S.; Zheng, C.; Zhang, X.; Emge, T. J.; Li, J., *J. Am. Chem. Soc.* **2011,** *133*, 4153-4155; (d) Hu, Z.; Tan, K.; Lustig, W. P.; Wang, H.; Zhao, Y.; Zheng, C.; Banerjee, D.; Emge, T. J.; Chabal, Y. J.; Li, J., *Chem. Sci.* **2014,** *5*, 4873-4877; (e) Lan, A.; Li, K.; Wu, H.; Olson, D. H.; Emge, T. J.; Ki, W.; Hong, M.; Li, J., *Angew. Chem. Int. Ed.* **2009,** *48*, 2334-2338.

13. Hu, Z.; Huang, G.; Lustig, W. P.; Wang, F.; Wang, H.; Teat, S. J.; Banerjee, D.; Zhang, D.; Li, J., *Chem. Commun.* **2015,** *51*, 3045-3048.

14. Shustova, N. B.; Ong, T.-C.; Cozzolino, A. F.; Michaelis, V. K.; Griffin, R. G.; Dincă, M., *J. Am. Chem. Soc.* **2012,** *134*, 15061-15070.

15. Hu, Z.; Lustig, W. P.; Zhang, J.; Zheng, C.; Wang, H.; Teat, S. J.; Gong, Q.; Rudd, N. D.; Li, J., *J. Am. Chem. Soc.* **2015,** *137*, 16209-16215.

16. (a) Ji, M.; Lan, X.; Han, Z.; Hao, C.; Qiu, J., *Inorg. Chem.* **2012,** *51*, 12389-12394; (b) Li, L.; Zhang, S.; Xu, L.; Han, L.; Chen, Z.-N.; Luo, J., *Inorg. Chem.* **2013,** *52*, 12323-12325.

17. Gong, Q.; Hu, Z.; Deibert, B. J.; Emge, T. J.; Teat, S. J.; Banerjee, D.; Mussman, B.; Rudd, N. D.; Li, J., *J. Am. Chem. Soc.* **2014,** *136*, 16724-16727.

18. Nimmermark, A.; Öhrström, L.; Reedijk, J., *Z. Kristallogr.* **2013,** *228*, 311-317.

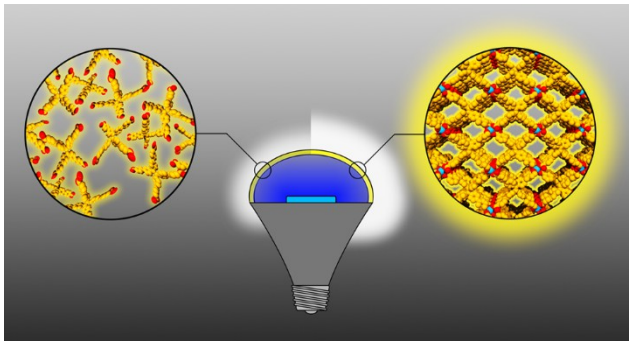

For Table of Contents Only:

Synopsis:

We discuss the rational design of highly efficient luminescent metal-organic frameworks (LMOFs) by immobilizing strongly emissive chromophores into their structures. This process presents a new approach to significantly improve their luminescence quantum yield, thermal stability and systematically tune their emission energy and color through the inclusion of secondary ligands or guest molecules. The exceptionally high performance of these LMOFs make them promising candidates as rare-earth free phosphors for energy-efficient lighting applications.